Journal of
Materials Chemistry C

PAPER

View Article Online
View Journal | View Issue

Published on 08 January 2014. Downloaded by Institute of Physics, CAS on 23/04/2014 08:52:30.

Cite this: *J. Mater. Chem. C*, 2014, **2**, 2417

Morphology inducing selective plasma etching for AlN nanocone arrays: tip-size dependent photoluminescence and enhanced field emission properties

Weijie Sun, Yunlong Li, Yang Yang, Yunming Li, Changzhi Gu* and Junjie Li*

Received 14th November 2013
Accepted 6th January 2014

DOI: 10.1039/c3tc32240h

www.rsc.org/MaterialsC

The bottom-up growth method has been the main way to form various AlN nanostructures, but there still exists many problems in the lack of control and non-uniformity. Here, we adopt a firstly top-down plasma etching method to easily fabricate large-area AlN nanocone arrays on magnetron sputtered (002) AlN films, and the unique, pebble-like array morphologies of the AlN films surface greatly induce the whole selective plasma etching process without any masked process. The as-formed AlN nanocones not only keep the crystalline oriented (002) and microstructure of the original AlN film, but also have a good uniformity and controllability in the height and density, as well as the tip-size. These AlN nanocone arrays exhibited an intense broad ultraviolet emission, centered at 3.26 eV and excellent field emission properties, especially showing a tip-size dependent photoluminescence and field emission properties that were remarkably enhanced with decreasing the nanocone tip-size. Our results provide a promising route for the controllable fabrication of AlN nanostructures and practical application of AlN-based various nanodevices in optoelectronics and vacuum-nanoelectronics.

1. Introduction

The group III-nitride compounds have stimulated significant research interest, due to their unique properties and significant applications, such as optoelectronic devices in the visible and ultraviolet region.[1] Among these compounds, aluminum nitride (AlN) exhibits high thermal conductivity, good electrical resistance, low dielectric loss, excellent mechanical strength and chemical stability.[2,3] It is also known that AlN has a small electron affinity value, ranging from the negative to 0.6 eV, which means that electrons can be easily extracted from the surface to a vacuum when an electric field is applied, thereby giving rise to a large field emission current density that is very attractive for field emission applications.[4] In addition, AlN exhibits the largest direct band gap, of about $\sim$6.2 eV, among the hexagonal group III nitrides and it is thus crucial to produce solid-state light emitting devices.[5] In particular, AlN nanostructures have shown more novel physical and chemical properties than bulk AlN materials, such as small electron affinity, strong piezoelectricity, high surface acoustic wave (SAW) velocity and a tunable band gap, which are essential for applications in field emitters, flexible pulse-wave sensors and ultraviolet nanolasers.

Recently, various AlN nanostructures such as nanobelts,[5] nanotubes,[6] nanocones[7,8] and hierarchical comb-like structures,[9] have been synthesized by different methods. Among these nanostructures, AlN nanocones have emerged as a new kind of one-dimensional nanostructures, that is superior to other nanostructures in some aspects. For instance, it is found that the nanocones are better potential candidates for scanning probes and field emitters, due to their radial rigidity, which eliminated the poor signals and noise caused by mechanical or thermal vibration.[10,11] Up until now, the reported AlN nanocones or similar nanostructures have mainly been formed by bottom-up growth methods,[12–15] but there still exists many problems in the growth process, such as lack of control and non-uniformity, and thus the fabrication of large-area, high-quality and controllable well-aligned AlN nanocone arrays has still remained as one of the foremost challenges, due to technological limitations. In addition, owing to its large direct band gap, some researchers have studied the photoluminescence (PL) properties of AlN nanostructures, however, the dependence of the PL properties on the geometry-size of the AlN nanostructure and related mechanism are scarcely discussed, so far.

In this work, we adopted firstly a top-down method of maskless plasma etching, to fabricate high-aligned AlN nanocone arrays with an ordered orientation, controlled density and uniform cone angle on a (002) AlN film, by using a hot filament chemical vapor deposition (HFCVD) system. The as-fabricated and highly-aligned AlN nanocone arrays retains the unchanged

Beijing National Laboratory for Condensed Matter Physics, Institute of Physics, Chinese Academy of Science, Beijing 100080, China. E-mail: jjli@aphy.iphy.ac.cn; czgu@iphy.ac.cn; Fax: +86-10-82648198; Tel: +86-10-82649097

Published on 08 January 2014. Downloaded by Institute of Physics, CAS on 23/04/2014 08:52:30.

crystalline orientation (002) and microstructure of the original AlN film, which can be served as a promising candidate for field emission (FE) and light emitters with enhanced properties induced by the multiple-nanotips geometry, due to their low electron affinity and large direct band gap. Compared with the previously reported bottom-up growth method of the AlN nanocones,[8] this top-down plasma etching method to fabricate an AlN nanocone shows clear superiority, such as the controllable morphology, good uniformity, large-area and high-throughput fabrication of the nanocone arrays, providing a very simple and advantageous fabrication approach. In addition, the process of the highly-aligned AlN nanocone arrays on the silicon substrates is amenable to the current technology for the fabrication of Si-based microelectronic devices. The subsequent characterizations of the FE and PL reveal that these AlN nanocone arrays possess a broad blue emission band and good FE properties, that can be tuned by the tip-size and density of the AlN nanocone, suggesting great potential applications in optoelectronics and field emission nanodevices.

2. Experimental

2.1 Preparation of (002) AlN films

The (002) AlN films were deposited on n-type (100)-oriented silicon substrates in a radio frequency (RF) magnetron sputtering system. Aluminum, with 99.99% purity, was used as the sputtering target. Prior to loading into the sputtering chamber, the substrate was cleaned by dipping in a dilute solution of 4% HF, for 60 s, to remove the chemical surface oxide layer. Degreasing was carried out by ultrasonic-assisted cleaning in acetone and methanol. Once the base gas pressure of the chamber reached 1×10^{-4} Pa, a gas flow mixture of high-purity N_2 and Ar was maintained in the chamber with a flow ratio of about 60 : 40. The total gas pressure was kept at 0.75 Pa during the sputtering process. The sputtering power and substrate temperature were kept at 120 W and 700 °C, respectively.

2.2 Fabrication of AlN nanocone arrays

After the growth process, the (002)-oriented AlN film with a thickness of about 800 nm was placed into the HFCVD chamber with a direct current (dc) negative bias voltage for the fabrication of the AlN nanocone arrays, and CH_4 and H_2 were used as the etching gas. The fabrication process was based on ion sputtering, in which the Ta filament in the HFCVD system was heated to about 2100 °C, and a negative bias voltage of 300 V was applied to the substrate to generate the glow discharge and ion sputtering. The substrate temperature was monitored using a thermocouple and modulated by changing the distance between the filament and substrate. The other experimental conditions for the AlN nanocone arrays formation were set as follows: the flow rate of CH_4 and H_2 was, respectively, in the range 1–5 sccm and 99–95 sccm, to obtain a CH_4 concentration of 1–5%, and the gas pressure was kept at 20 Torr, while the glow discharge current was 150 mA, and the duration of the ion sputtering was 1–2 h.

2.3 Characterization

The surface morphology of the AlN film was characterized by a scanning electron microscope (SEM), and the X-ray diffraction (XRD) measurement was used to prove that high-quality (002)-oriented AlN films were formed under the above-mentioned experimental conditions. In addition, the AlN nanocone arrays were characterized by a transmission electron microscope (TEM) and Energy Dispersive X-Ray Spectroscopy (EDX) to observe their microstructures and components. The field emission properties for the AlN nanocone array measurements were performed by using a conventional parallel-plate field configuration with an anode-to-sample spacing of 200 μm (using glass fibers as spacers for all tests) under a vacuum of 2×10^{-6} Pa. The PL measurements were carried out at room temperature, using a HR800 spectrometer with a 325 nm excitation of a He–Cd laser.

3. Results and discussion

The AlN films deposited on the (100)-oriented silicon wafer by the RF magnetron sputtering method, were used as substrates for the fabrication of AlN conical nanostructure, as shown in Fig. 1a. It can be seen that the as-deposited AlN films display a pebble-like morphology with a uniform grain size of about 20 nm in diameter, reflecting the typical surface character of (002)-oriented AlN films, that is favorable for further fabrication of the conical structure. After plasma etching for about 1 h, uniform AlN nanocone arrays were achieved on the AlN film. As shown in Fig. 1b, the SEM image of aligned AlN nanocone arrays are presented, having a high density of the nanocone of about 1×10^9 cm^{-2} and a high aspect ratio. Moreover, from Fig. 1c, we can see that the length of an individual nanocone is about 600 nm with a cone angle approximately of 17°, which is advantageous for tip-enhanced emission applications. Fig. 1d

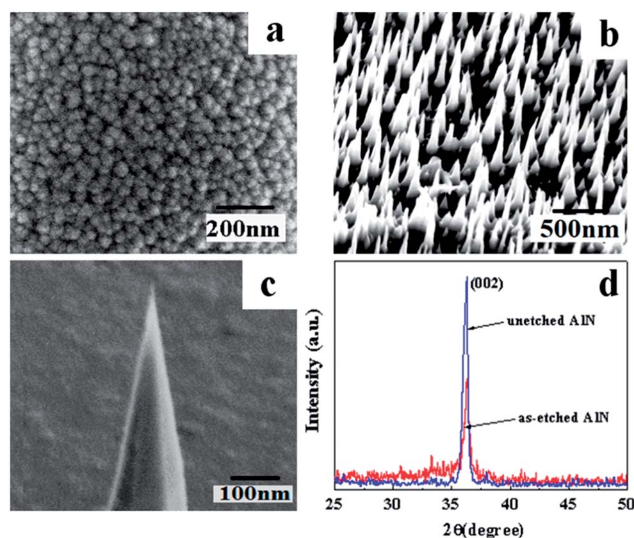

Fig. 1 SEM images of (a) original (002)-oriented AlN film, (b) as-formed AlN nanocone arrays, and (c) a individual nanocone. (d) XRD measurement results of (002) AlN film before and after etching.

 This journal is © The Royal Society of Chemistry 2014

Published on 08 January 2014. Downloaded by Institute of Physics, CAS on 23/04/2014 08:52:30.

shows the XRD measurement results of the (002) AlN film before and after plasma etching, in which a strong diffraction peak appears at about a 2θ value of 36°, indicating a highly (002)-oriented character for the as-formed AlN films.[16] It was found that the intensity of the diffraction peak of the AlN films was reduced due to the plasma etching process, but its location at 2θ 36°was unchanged, verifying that the plasma etching has not greatly changed the microstructure of the (002) AlN film. These results indicated that the as-formed AlN nanocone still remained most of its intrinsic properties, though the plasma etching might introduce defects.

To further determine the detailed crystalline structure of the AlN nanocone, a HRTEM measurement was employed to investigate the samples. A typical TEM image of a single AlN nanotip is shown in Fig. 2a, displaying a tiny apex radius and smooth surface. An amorphous layer, of several nanometers is also observed on the side-wall, which is very likely be a very thin amorphous AlN layer that originates from redeposition during the etching process. Furthermore, no masked particles are found on the cone tip, also testifying a maskless plasma etching fabrication process. Fig. 2b shows a HRTEM image of the local region of the AlN nanocone, finding that the AlN nanocone has clear main atom lattice fringes and the distance spacing between the adjacent (002) plane is 0.25 nm, which is in agreement with the results of the XRD measurement and presents the growth structure with a preferential growth direction along the (002) direction. In addition, the SAED pattern shown in Fig. 2c indicates that a crystal phase of the AlN nanotip can be obtained, in which a preferred orientation is already seen from the arcing of the (002) diffraction spots around the growth axis, according to the occurring diffraction rings.[17] Thus, it can be seen that according to this SAED pattern, with very intense diffraction spots, the AlN nanocone is obviously typical of a polycrystalline microstructure, with well defined crystallite. Finally, the local EDX spectroscopy analysis results in Fig. 2d indicated that the as-formed nanocone was composed of Al and N elements, corresponding to AlN, and the O element content may be attributed to the etching process.

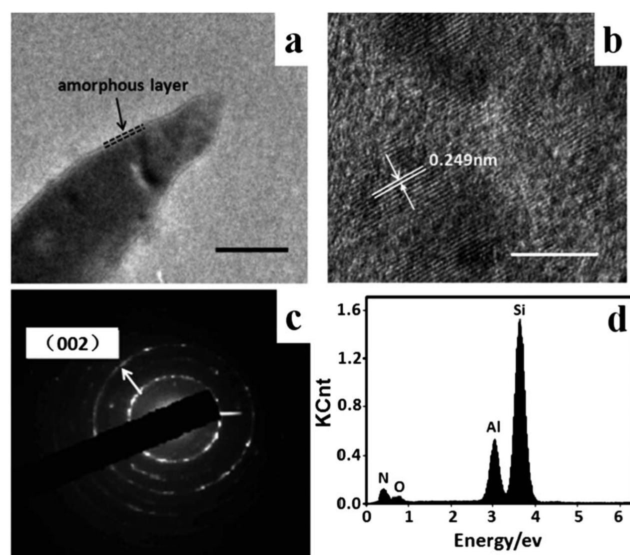

Fig. 2 TEM, SAED and EDX analyses of a typical AlN nanocone: (a) TEM image of a single AlN nanotip. Scale bar, 40 nm. (b) HRTEM image. Scale bar, 5 nm (c) SAED patterns and (d) EDX spectrum corresponding to the top region of AlN nanocone.

Based on the above results, together with the reaction principles of the maskless selective plasma etching, a top-down formation mechanism for the AlN nanocone has been proposed, as illustrated in Fig. 3. Under the same etching condition and with the same substrate materials, a roughness surface is more favorable to form a cone-shape structure than a smooth surface, which is an effect of the morphology inducing plasma etching. During the plasma etching, the incident energetic ions should collide more frequently with the concave sections than the convex sections.[18] It should be noted that the particle movement is complicated and unpredictable, due to the existence of the sheath field and the additional three-dimensional (3D) electric fields of random surface nanostructures, which indicates only a statistical method can be employed to provide definite evidence of the as-obtained experimental results. In Fig. 2a, a pebble-like grain can be considered as a hillock, and the different sputtering rates for the different regions of the hillock are very different. If the relation of $\bar{E} > E_{th}$ ($\bar{E}$: average ion energy; and E_{th}: sputtering threshold energy) is satisfied, a sputtering of the substrate will occur. The target atoms were not usually sputtered from the exact hitting spots of the incident ions, and target atoms near the hitting spots will be sputtered out "down-stream", due to a cascade-collision for low energy sputtering.[19] The sputtering rate of the cone tip is less than that of the cone bottom ($\nu_{top} < \nu_{bottom}$), and for the cones with a smaller cone angle this effect becomes more apparent. At

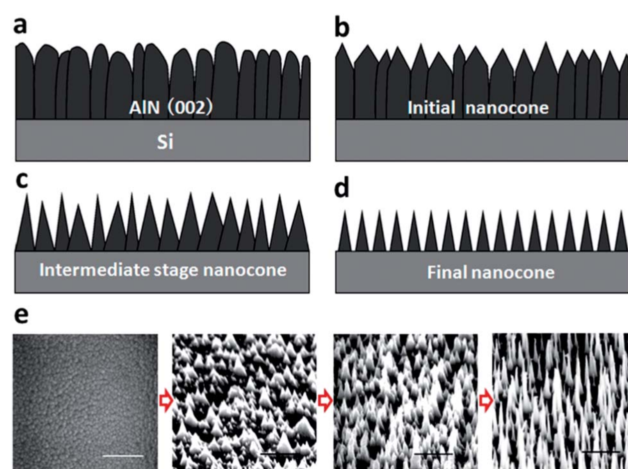

Fig. 3 Illustration of morphology inducing maskless plasma etching to fabricate AlN nanocone arrays. (a) (002) AlN film with surface morphology of pebble-like grains and columnar-like cross-section before plasma etching, (b) etching initial stage, the top of columnar-like structure become the low conical shape due to pebble-like morphology inducing selecting etching, (c) and (d) after etching duration, the size and shape of nanocone is developed to form finally discrete and uniform nanocone arrays. (e) Real SEM morphologies of AlN films and nanocone arrays corresponding to each stage of plasma etching process from (a) to (d). Scale bar, 500 nm.

Published on 08 January 2014. Downloaded by Institute of Physics, CAS on 23/04/2014 08:52:30.

last, a certain static equilibrium among the etching of different parts will be reached, and the cones with a relative height and cone angle will be developed, as illustrated in Fig. 3b–d. The actual SEM images of the as-formed AlN nanocone arrays are shown in Fig. 3e with etching evolution, demonstrating the above mechanism of the morphology inducing maskless plasma etching. Therefore, the pebble-like surface structure of the (002) AlN film morphologically induced the plasma etching, to procure the initial formation of the nanocone structure, which produced an enhanced ion sputtering effect on the pebble-like grain bases, and the nanocone structure, with a larger height and smaller cone angle, will be developed by further sputtering. During the formation of surface nanocones, the methylic ions play a major role in determining the etching efficiency, due to their much higher mean ion energies than that of the H^+ ions.[18] The H^+ ions, with lower energy, will result in a poor etching efficiency, but it is helpful for developing the initial surface roughness. In spite of that, a proper gas flow ratio (CH_4/H_2) should be carefully controlled during the etching process; a higher gas flow rate will result in an excessive etching. In addition, other etching parameters, such as the gas pressure, bias current and etching time have an obvious effect on the morphology of the as-formed AlN nanocone, which also has close relations with the mean free path and the mean energy of the ions. Among these etching parameters, a lower gas pressure can increase the mean free path of the ions and hence obtain a higher ion mean energy to improve the etching efficiency, and thus a proper gas pressure is helpful to form the nanocone with a high aspect ratio. A higher bias current can greatly enhance the etching efficiency, due to an increased ion current density and stable ion mean energy, and thus a reasonable control in the bias current is a very effective way to tune the different morphologies of the AlN nanocone. Finally, under optimal etching parameters, controlling the etching time becomes of great importance to a perfect etching result, by which we can obtain different morphologies of the AlN nanocone, including the density, height and tip angle of the nanocone.

AlN nanocone samples, with different tip-sizes from ~50 nm to ~10 nm, were selected to investigate thoroughly the effect of the tip-size on the PL properties of the AlN nanocone. Fig. 4 presents the PL spectra of the AlN film and nanocone arrays under the excitation wavelength of 325 nm. Compared with the AlN film, the AlN nanocones show a great enhancement in the PL intensity, and then a reduction in the tip-size of the AlN nanocone can lead to a continuous improvement of the PL intensity. Despite the changes in the relative intensity of the PL bands, two broad PL bands are still centered at 380 nm (3.26 eV) and 460 nm (2.7 eV), respectively, as shown in Fig. 4. This means that the emission originates the same electron transition in the series of samples with the AlN film. Obviously, these two PL bands cannot be attributed to the band-to-band transitions, since AlN exhibits a wide direct band gap of ~6.2 eV, corresponding to the phonon–exciton emission band around 200 nm. Also, the PL bands observed in the range 2–4 eV are generally attributed to the oxygen-related defects in the lattice structure of AlN.[9] Two oxygen atoms (O_N) substituting two nitrogen atoms and resulting in an N vacancy (V_N), lead to the

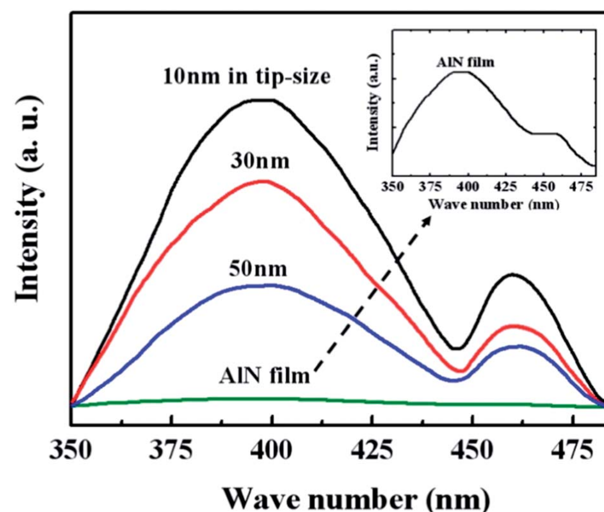

Fig. 4 PL curves of AlN film and nanocone with various apex radiuses: 10 nm, 30 nm, 50 nm, and an inserted and enlarged PL spectrum of AlN film.

different defect levels of the O_N–V_{Al} complex.[20] Two prominent features in Fig. 4 are worthy to be addressed here. The first one is the significant enhancement of the PL bands for the AlN nanocone arrays, compared with that of the AlN film. The enhanced PL band centered at 380 nm has been observed in AlN nanowires, nanotips and nanopyramids.[13–15] According to classification of Berzina *et al.*, the 380 nm band originates from the excitations of the O_N–V_{Al} complex to the separated O_N ion level.[21] On the other hand, the relatively weak band around 460 nm has also been observed in other AlN nano-materials, such as nanocrystal and nanotubes, which is attributed to the vacancies of N.[22] Secondly, it is striking to find that the PL intensities increase with the decrease of the apex radius of the cones, especially for the nanocones with an average apex radius of 10 nm, of which the PL intensity is thirty times stronger than that of the AlN film. It is generally accepted that the PL intensity of semiconductors increases when their size decreases to the nanometer scale, due to the increasing surface defects and oxygen impurities that increase the recombination rate of the phonon-induced electron–hole pairs.[23] Torchynska has demonstrated that the PL intensity increases while decreasing the grain size of Si nano-crystallites.[24] The enhancement of the 380 and 460 nm PL bands for the AlN nanocone arrays may be associated with the increased luminance centers that arise from the etching process. The longer the etching time, the smaller the nanocones, and the higher defect density on the cone surface. In addition, the surface defects of the cones also improve the light excitation efficiency.[25] The nanocone structures assist the photons with multiple opportunities to escape from the wafer surface and redirect the photons which are originally emitted out of the escape cone back into the escape cone.[26] The intense PL emission in the range 2–4 eV indicates that the well-aligned AlN cones would have potential applications in light emission nanodevices.

To further evaluate the feasibility of applying AlN in vacuum nanoelectronic fields, we have measured the FE properties of

 This journal is © The Royal Society of Chemistry 2014

Published on 08 January 2014. Downloaded by Institute of Physics, CAS on 23/04/2014 08:52:30.

AlN nanocone arrays with various cone densities, as shown in Fig. 5. Three kinds of nanocone samples were selected from the many samples used as field emitters, which have a similar morphology of cone height and cone angle, but different cone densities, corresponding to 1×10^9, 5×10^8 and 8×10^7 cm^{-2}, respectively. From the *J–E* curve of the AlN nanocone arrays and film (Fig. 5a), we found that the emission current density of the nanocone array is greatly higher than the film at the same applied electric field, which is mainly attributed to the nanotip-geometrical enhancement effect of the nanocones. In order to compare the FE capability of the above three kinds of nanocone arrays with different densities, their turn-on fields (defined as turn-on field for 10 μA cm^{-2}) were found to be 5.6V μm^{-1}, 3.2 V μm^{-1}, and 7.9 V μm^{-1}, respectively. The current densities of these nanocone arrays were measured to be 145 μA cm^{-2}, 352 μA cm^{-2}, and 22 μA cm^{-2}, when the electric field was kept at 8 V μm^{-1}. It is clearly indicated that the AlN nanocone array sample with a density of 5×10^8 cm^{-2} has the best FE characteristics among the three samples with different densities. The results indicate that the local field electron emission ability can be observably increased with increasing the nanocone density. More nanocones may provide a large number of emitting sites to contribute to the electron tunneling enhancement for electron emission. Nevertheless, too high a nanocone distribution will bring field shield effects, that result in the reduction of the FE property. Thus, we can conclude that a proper AlN nanocone density can enhance greatly the electron emission property. In addition, compared with the reported results of as-grown AlN nanostructures,[27–29] the AlN nanocone array fabricated here by maskless plasma etching has a better FE property, with improved low turn-on field and a high current density. A good morphology control and high uniformity of the as-formed AlN nanocone arrays in this work can effectively optimize the emission site density and emission stability, and their high aspect ratio and tiny tips may greatly increase the field enhancement factor for improving the electron emission ability. In addition to the density, the apex angle and conductivity of the nanocone have a considerable influence on their FE properties. In this work, we were concerned primarily with the effect of the nanocone density on the FE properties, because the FE ability is greatly dependent on the density of the emission site, that is determined mainly by the density of the nanocone.

The corresponding Fowler–Nordheim (FN) plots of the AlN nanocone arrays with different densities and the AlN film are shown in Fig. 5b. The linearity of the four curves indicated that their FE process follows FN theory, and the measured current is apparently due to the FE. According to the FN equation, if we assumed a constant work function of 3.7 eV, the field enhancement factor of various densities of cone arrays could be estimated to be 286, 484, and 402, by the FN equation and FN plot slope, respectively.[30] These values imply that the 5×10^8 cm^{-2} nanocone array has a bigger field enhancement factor than that of the 1×10^9 and 8×10^7 cm^{-2} nanocone arrays. Otherwise, the emission stability was tested for about 1 h at a constant electric field. No visible degradation of the current density was observed. Therefore, our results proved that the as-fabricated AlN nanocone arrays have excellent and stable FE properties, and using plasma etching to fabricate an AlN nanocone is a promising route for the practical application of AlN-based field emitters.

4. Conclusions

In summary, vertically aligned AlN nanocone arrays with controllable densities and tip-sizes have been successfully fabricated by using a top-down plasma etching method. A morphology inducing selective plasma etching process was developed to fabricate lager-area AlN nanocone arrays without any masked process. The as-fabricated AlN nanocones showed a great enhancement in the PL and FE properties, depending on the tip-size of AlN nanocones. With decreasing apex radius of the cones, the PL intensities of AlN nanocone arrays were increased gradually, which was due to the formation of the high-density nanocone structures, with rich surface defects and oxygen impurities induced by plasma etching, that increases the recombination rate of the phonon-induced electron–hole pairs. The FE results indicate that the high densities and tip-effect of the AlN nanocone arrays lead to their good field emission ability, and more nanocones may provide a large number of emitting sites to contribute to the electron tunneling enhancement, but increasingly dense nanocones work against the increase of the FE, due to field shield effects. Therefore, this morphology inducing selective plasma etching method provides a very simple and effective approach to fabricate AlN

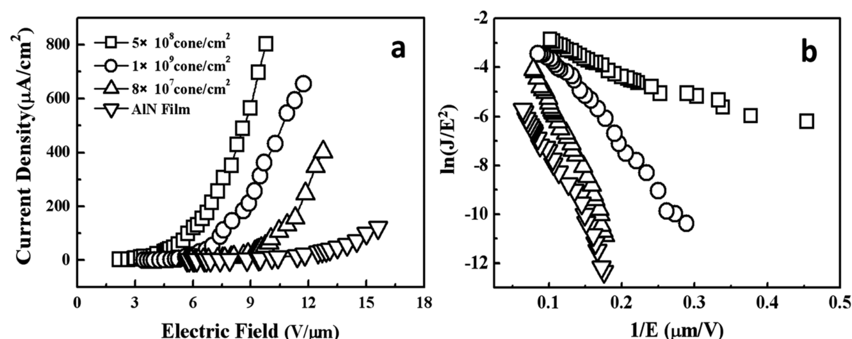

Fig. 5 Field emission *J–E* curve of AlN nanocone arrays with different densities (a) and corresponding to FN plots (b).

nanocone arrays with reliable control and uniformity, as well as a high-throughput, for further practical applications of AlN-based nanodevices in optoelectronics and the nanoelectronics field.

Acknowledgements

The authors acknowledge the National Natural Science Foundation of China (Grant no. 11174362, 91023041, 91323304, 51272278, 61390503), and the Knowledge Innovation Project of CAS (Grant no. KJCX2-EW-W02).

Published on 08 January 2014. Downloaded by Institute of Physics, CAS on 23/04/2014 08:52:30.

Notes and references

1 S. Nakamura and G. Fasol, *The Blue Laser Diode*, Springer, Heidellberg, 1997.
2 M. C. Benjamin, C. Wang, R. F. Davis and R. J. Nemanich, *Appl. Phys. Lett.*, 1994, **64**, 3288.
3 Y. Taniyasu, M. Kasu and T. Makimoto, *Nature*, 2006, **441**, 325.
4 C. Liu, Z. Hu, Q. Wu, X. Z. Wang, Y. Chen, H. Sang, J. M. Zhu, S. Z. Deng and N. S. Xu, *J. Am. Chem. Soc.*, 2005, **127**, 1318.
5 Y. B. Tang, H. T. Cong, Z. G. Zhao and H. M. Cheng, *Appl. Phys. Lett.*, 2005, **86**, 153104.
6 L. W. Yin, Y. Bando, Y. C. Zhu, M. S. Li, C. C. Tang and D. Golberg, *Adv. Mater.*, 2005, **17**, 110.
7 S. C. Shi, C. F. Chen, S. Chattopadhyay, Z. H. Lan, K. H. Chen and L. C. Chen, *Adv. Funct. Mater.*, 2005, **15**, 781.
8 Y. L. Li, C. Y. Shi, J. J. Li and C. Z. Gu, *Appl. Surf. Sci.*, 2008, **254**, 4840.
9 J. H. He, R. Yang, Y. L. Chu, L. J. Chou, L. J. Chen and Z. L. Wang, *Adv. Mater.*, 2006, **18**, 650.
10 G. Y. Zhang, X. Jiang and E. G. Wang, *Science*, 2003, **300**, 472.
11 Q. Wang, Z. L. Wang, J. J. Li, Y. Huang, Y. L. Li, C. Z. Gu and Z. Cui, *Appl. Phys. Lett.*, 2006, **89**, 063105.
12 W. M. Yim, E. J. Stofko, P. J. Zanzucchi, J. I. Pasnkove, M. Ettehberg and S. L. Gilbert, *J. Appl. Phys.*, 1973, **44**, 292.
13 C. Xu, L. Xue, C. Yin and G. Wang, *Phys. Status Solidi A*, 2003, **198**, 329.
14 S. C. Shi, C. F. Chen, S. Chattopadhyay, K. H. Chen, B. Ke, L. Chen, L. Trinkler and B. Berzina, *Appl. Phys. Lett.*, 2006, **89**, 163127.
15 J. Zheng, X. Song, B. Yu and X. Li, *Appl. Phys. Lett.*, 2007, **90**, 193121.
16 H. Okano, Y. Takahashi, T. Tanaka, K. Shibata and S. Nakano, *Jpn. J. Appl. Phys.*, 1992, **31**, 3446.
17 J. X. Zhang, Y. Z. Chen, H. Cheng, A. Uddin, S. Yuan, K. Pita and T. G. Andersson, *Thin Solid Films*, 2005, **471**, 336.
18 Q. Wang, C. Z. Gu, Z. Xu, J. J. Li, Z. L. Wang, X. D. Bai and Z. Cui, *J. Appl. Phys.*, 2006, **100**, 034312.
19 J. Zhou, I. T. Martin, R. Ayers, E. Adams, D. Liu and E. R. Fisher, *Plasma Sources Sci. Technol.*, 2006, **15**, 714.
20 S. Schweizer, U. Rogulis, J.-M. Spaeth, L. Trinkler and B. Berzina, *Phys. Status Solidi B*, 2000, **219**, 171.
21 B. Berzina, L. Trinkler, J. Sils and K. Atobe, *Radiat. Eff. Defects Solids*, 2002, **157**, 1089.
22 T. Xie, X. Y. Yuan, G. S. Wu, Y. Lin, X. X. Xu, G. W. Meng and L. D. Zhang, *J. Phys.: Condens. Matter*, 2004, **16**, 1639.
23 S. Bellucci, A. I. Popov, C. Balasubramanian, G. Cinque, A. Marcelli, I. Karbovnyk, V. Savchyn and N. Krutyak, *Radiat. Meas.*, 2007, **42**, 708.
24 T. V. Torchynska, *Phys. Status Solidi C*, 2007, **4**, 375.
25 D. W. Kim, H. Y. Lee, M. C. Yoo and G. Y. Yeom, *Appl. Phys. Lett.*, 2005, **86**, 052108.
26 C. B. Soh, B. Wang, S. J. Chua, K. X. Lin, J. N. Tan and S. Tripathy, *Nanotechnology*, 2008, **19**, 405303.
27 W. J. Qian, H. W. Lai, X. Z. Pei, J. Jiang, Q. Wu, Y. L. Zhang, X. Z. Wang and Z. Hu, *J. Mater. Chem.*, 2012, **22**, 18578–18582.
28 X. H. Ji, Q. Y. Zhang, S. P. Lau, H. X. Jiang and J. Y. Lin, *Appl. Phys. Lett.*, 2009, **94**, 173106–173108.
29 W. J. Qian, Y. L. Zhang, Q. Wu, C. Y. He, Y. Zhao, X. Z. Wang and Z. Hu, *J. Phys. Chem. C*, 2011, **115**, 11461–11465.
30 J. J. Li, C. Z. Gu, Q. Wang, P. Xu, Z. L. Wang, Z. Xu and X. D. Bai, *Appl. Phys. Lett.*, 2005, **87**, 143107–143109.

This journal is © The Royal Society of Chemistry 2014